Symplectic Solution for Size-dependent Contact Analysis

Lizichen Chen[a], C.W. Lim[a,b], Weiqiu Chen[a,c,d,*]

[a]Key Laboratory of Soft Machines and Smart Devices of Zhejiang Province, Department of Engineering Mechanics, Soft Matter Research Center, Zhejiang University, Hangzhou 310027, P.R. China

[b]Department of Architecture and Civil Engineering, City University of Hong Kong, Tat Chee Avenue, Kowloon, Hong Kong SAR, P.R. China

[c]Center for Soft Machines and Smart Devices, Huanjiang Laboratory, Zhuji 311816, P.R. China

[d]Faculty of Mechanical Engineering and Mechanics, Ningbo University, Ningbo 315211, P.R. China

Abstract: A novel symplectic framework suitable for size-dependent contact analysis has been established. The governing equations in symplectic form are derived for the contact between a no-slip rigid punch and a finite-sized plane with horizontal exponential material gradient. The dual Hamiltonian transformation of a quasi-Hamiltonian operator with asymmetric lower-left block is constructed. Analytical eigen-solutions are obtained that lead to derivation of the coefficients in symplectic expansion via Hamiltonian mixed energy variational principle. The unique formulation of symplectic expansion in principle stems from the specific distribution of eigenvalues. Local phase transition is observed and analysis shows that size effects originate from the existence of real eigenvalues. A typical numerical example is presented to illustrate the efficiency of this symplectic approach. This new approach to contact analysis lays a solid theoretical foundation for material characterization that utilizes high-throughput testing methodologies and functionally graded specimens.

Keywords: symplectic framework; size-dependent contact; horizontal exponential gradients; local phase transition; quasi-Hamiltonian operator

* Corresponding author. Tel./Fax: 85-571-87951866; E-mail: chenwq@zju.edu.cn.

1. Introduction

The recent advent of materials at micro- and nano-scales [1,2] through extensive research not only has unveiled the unique properties of minute specimens but also has made significant advances in device miniaturization. Being a typical representative device in this regard, the micro-electro-mechanical system (MEMS) requires more meticulous considerations in the design and applications because of the unique size-dependent and surface effects that critically influence its mechanical properties [3,4]. Moreover, numerous micro-scale friction and contact issues arise during the operation of MEMS [5], thus posing great challenges to stability and reliability of the system. To better understand material properties at micro- and nano-scales and to accurately predict the special mechanical behaviors, many scholars have developed higher-order continuum mechanics models such as the couple stress theory [6-8], and the nonlocal theory [9] by introducing new internal, size-dependent material parameters [10-12]. The presence of couple stresses results in the asymmetric Cauchy stress tensors, and violation of the reciprocal theorem of shear stresses. For this reason, Yang et al. [13] then established a modified couple stress theory for isotropic materials by neglecting the antisymmetric component.

There exist many common methods such as integral transform and Green's function in the theoretical analysis of statics and dynamics of mechanical systems at minute scales. Notably, Muki and Sternberg [14] studied the response of flat punch indentation involving couple-stresses by dual integral equations. In a series of research works, Zisis and his collaborators summarized some fundamental techniques of two-dimensional contact problems with couple stresses, considering frictionless contact problems of a homogeneous elastic half-plane under a rigid indenter in the plane-strain state [15]. They also reported complete and receding contact problems with tilted flat punch [16], frictionless contact problems under cylindrical and wedge indenters [17], and contact problems in a layered system [18,19]. In terms of multi-field coupling, they also explored the thermoelastic contact problem with a flat indenter [20]. Wang and his collaborators focused on three-dimensional spherical rigid indenters by analyzing the impact of material characteristic length, Poisson's ratio, and film thickness on contact behaviors [21,22]. Based on micro- and nano-contact mechanics, some advanced instruments such as nanoindentors and atomic force microscopes (AFM) were proposed [23,24]. These instruments play a crucial role in characterizing material performance, and in measuring parameters such as

elastic modulus, hardness, and fracture toughness of advanced materials [25].

Nevertheless, research works on size-dependent contact analyses that focus on inhomogeneous media have been very limited. To a certain extent, the inherent complexity of the size-dependent effects puts forward a challenge for us to propose a novel framework to address the issues based on a new symplectic methodology. The early works of symplectic framework was due to Zhong and his associates [26,27] for elasticity. They further generalized it to include a model with couple stresses [28] which involves three Mindlin stress functions and its corresponding strain as the dual variables. However, this formulation is not efficient for the contact problems that feature mixed boundary conditions. The authors recently conducted contact analyses of finite-sized horizontally graded [29] and laminated [30] planes with multi-field couplings based on symplectic elasticity, laying a foundation for the theoretical derivations presented in this paper.

A novel symplectic framework for the contact analysis of a no-slip rigid punch acting on the surface of a finite-sized plane with an exponential material gradient in the horizontal direction is proposed in this article. The dual Hamiltonian transformation of a quasi-Hamiltonian operator is derived via the governing equations in symplectic forms. Zero eigenvalue and general eigenvalues along with the corresponding eigen-solutions are established analytically in Sections 2.1 and 2.2, respectively, which facilitate the symplectic expansion for a complete solution in Section 2.3. The local phase transition observed in the distributions of eigenvalues is analyzed in Section 3.1, which provides an interpretation for the phenomenon of size effects. A simple numerical example is presented in Section 3.2. The paper ends with concluding remarks presented in Section 4.

2. Theory, Modeling and Formulation

A flat punch applied to the surface of a finite-sized functionally graded plane as illustrated in Fig. 1 is considered. The plane is isotropic with Young's modulus E, Poisson's ratio ν, and material characteristic length ℓ. Without the loss of generality, we assume E varies exponentially along the x-direction, i.e. $E(x) = E_0 \mathrm{e}^{\beta x}$, while the other material parameters remain constant, where E_0 represents the reference Young's modulus at the coordinate origin; and β

is the material gradient index. To elucidate, the material characteristic length features the size of the microstructure or microdefects present within the material, which is essential when the material size scaling down to the order of microscales.

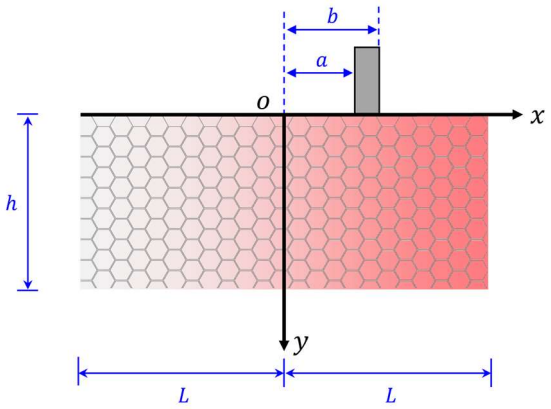

Fig. 1. A flat punch acting on the surface of a finite-sized plane with horizontally graded material property.

For the case of plane strain, the two-dimensional constitutive equations are in the form of

$$\begin{cases} \varepsilon_{xx} = \dfrac{\partial u_x}{\partial x} = \dfrac{1+\nu}{E}\left[(1-\nu)\sigma_{xx} - \nu\sigma_{yy}\right] \\ \varepsilon_{yy} = \dfrac{\partial u_y}{\partial y} = \dfrac{1+\nu}{E}\left[(1-\nu)\sigma_{yy} - \nu\sigma_{xx}\right] \\ \varepsilon_{xy} = \varepsilon_{yx} = \dfrac{1}{2}\left(\dfrac{\partial u_x}{\partial y} + \dfrac{\partial u_y}{\partial x}\right) = \dfrac{1+\nu}{2E}\left(\sigma_{xy} + \sigma_{yx}\right) \\ \chi_{xz} = \dfrac{\partial \omega_z}{\partial x} = \dfrac{1}{2}\dfrac{\partial}{\partial x}\left(\dfrac{\partial u_y}{\partial x} - \dfrac{\partial u_x}{\partial y}\right) = \dfrac{1+\nu}{2E\ell^2} m_{xz} \\ \chi_{yz} = \dfrac{\partial \omega_z}{\partial y} = \dfrac{1}{2}\dfrac{\partial}{\partial y}\left(\dfrac{\partial u_y}{\partial x} - \dfrac{\partial u_x}{\partial y}\right) = \dfrac{1+\nu}{2E\ell^2} m_{yz} \end{cases} \tag{1}$$

where σ_{ij}, ε_{ij}, m_{ij}, and χ_{ij} are the stress, strain, couple stress, and curvature components, respectively; u_x and u_y are the displacement components in the x- and y-directions, respectively; ω_z is the rotation in the normal direction. Without considering body forces, Eq. (1) and the equilibrium equations are expressed in the form of

$$\begin{cases} \dfrac{\partial u_x}{\partial y}=\dfrac{\partial u_y}{\partial x}-2\omega_z \\ \dfrac{\partial u_y}{\partial y}=\dfrac{1+\nu}{E}\left[(1-\nu)\sigma_{yy}-\nu\sigma_{xx}\right] \\ \dfrac{\partial \omega_z}{\partial y}=\dfrac{1+\nu}{2E\ell^2}m_{yz} \\ \dfrac{\partial \sigma_{yx}}{\partial y}=-\dfrac{\partial \sigma_{xx}}{\partial x} \\ \dfrac{\partial \sigma_{yy}}{\partial y}=-\dfrac{\partial \sigma_{xy}}{\partial x} \\ \dfrac{\partial m_{yz}}{\partial y}=-\dfrac{\partial m_{xz}}{\partial x}+\sigma_{yx}-\sigma_{xy} \end{cases} \tag{2}$$

which can be simplified by introducing $\hat{\sigma}_{ij}=\sigma_{ij}\mathrm{e}^{-\beta x}$ and $\hat{m}_{ij}=m_{ij}\mathrm{e}^{-\beta x}$, as

$$\frac{\partial}{\partial y}\mathbf{I}_6\boldsymbol{f}=\boldsymbol{\mathcal{H}}\boldsymbol{f} \tag{3}$$

where $\mathbf{I}_n$ is a nth-order identity matrix; $\boldsymbol{f}=[\boldsymbol{q},\boldsymbol{p}]^{\mathrm{T}}=[u_x,u_y,\omega_z,\hat{\sigma}_{yx},\hat{\sigma}_{yy},\hat{m}_{yz}]^{\mathrm{T}}$ is the full state vector; and $\boldsymbol{\mathcal{H}}$ is a quasi-Hamiltonian operator

$$\boldsymbol{\mathcal{H}}=\left[\begin{array}{ccc:ccc} 0 & \dfrac{\partial}{\partial x} & -2 & 0 & 0 & 0 \\ -\dfrac{\nu}{1-\nu}\dfrac{\partial}{\partial x} & 0 & 0 & 0 & \dfrac{(1+\nu)(1-2\nu)}{E_0(1-\nu)} & 0 \\ 0 & 0 & 0 & 0 & 0 & \dfrac{1+\nu}{2E_0\ell^2} \\ \hdashline -\dfrac{E_0}{1-\nu^2}\left(\dfrac{\partial^2}{\partial x^2}+\beta\dfrac{\partial}{\partial x}\right) & 0 & 0 & 0 & -\dfrac{\nu}{1-\nu}\left(\dfrac{\partial}{\partial x}+\beta\right) & 0 \\ 0 & -\dfrac{2E_0}{1+\nu}\left(\dfrac{\partial^2}{\partial x^2}+\beta\dfrac{\partial}{\partial x}\right) & \dfrac{2E_0}{1+\nu}\left(\dfrac{\partial}{\partial x}+\beta\right) & \left(\dfrac{\partial}{\partial x}+\beta\right) & 0 & 0 \\ 0 & -\dfrac{2E_0}{1+\nu}\dfrac{\partial}{\partial x} & -\dfrac{2E_0\ell^2}{1+\nu}\left(\dfrac{\partial^2}{\partial x^2}+\beta\dfrac{\partial}{\partial x}\right)+\dfrac{2E_0}{1+\nu} & 2 & 0 & 0 \end{array}\right]$$

which can be further expressed as $\boldsymbol{\mathcal{H}}=\left[\begin{array}{c:c}\mathbf{A}&\mathbf{B}\\ \hdashline \mathbf{C}&\mathbf{D}\end{array}\right]$, with $\mathbf{A}=-\lim\limits_{\beta\to 0}\mathbf{D}^{\mathcal{T}}$, $\mathbf{B}=\mathbf{B}^{\mathcal{T}}$, and $\lim\limits_{\beta\to 0}\mathbf{C}=\lim\limits_{\beta\to 0}\mathbf{C}^{\mathcal{T}}$ (i.e., $\mathbf{C}\neq\mathbf{C}^{\mathrm{T}}$ in general), where $(\cdot)^{\mathcal{T}}$ represents the adjoint transpose of an operator matrix. Additionally, the supplementary equations can be derived as

$$\hat{\sigma}_{xy}=\frac{2E_0}{1+\nu}\left(\frac{\partial u_y}{\partial x}-\omega_z\right)-\hat{\sigma}_{yx},\quad \hat{\sigma}_{xx}=\frac{E_0}{1-\nu^2}\frac{\partial u_x}{\partial x}+\frac{\nu}{1-\nu}\hat{\sigma}_{yy},\quad \hat{m}_{xz}=\frac{2E_0\ell^2}{1+\nu}\frac{\partial \omega_z}{\partial x} \tag{4}$$

Furthermore, the dual Hamiltonian transformation is proved through integration by parts,

together with the homogeneous boundary conditions at $x=\pm L$: $\hat{\sigma}_{xy}=0$, $\hat{\sigma}_{xx}=0$, and $\hat{m}_{xz}=0$, which reads

$$\langle \boldsymbol{f}_1, \mathcal{H}\boldsymbol{f}_2 \rangle = \langle \boldsymbol{f}_2, \mathcal{H}\boldsymbol{f}_1 \rangle - \beta \left\langle \boldsymbol{f}_1^*, \boldsymbol{f}_2^* \right\rangle \tag{5}$$

where the subscript 1 or 2 denotes a specified state vector; $\boldsymbol{f}^* = [u_x, u_y, \omega_z, \hat{\sigma}_{xx}, \hat{\sigma}_{xy}, \hat{m}_{xz}]^{\mathrm{T}}$ is the dual full state vector. The symplectic inner product is defined as

$$\langle \boldsymbol{f}_1, \boldsymbol{f}_2 \rangle = \int_{-L}^{L} \boldsymbol{f}_1^{\mathrm{T}} \mathbf{J} \boldsymbol{f}_2 \mathrm{d}x = \int_{-L}^{L} (u_{x1}\hat{\sigma}_{yx2} + u_{y1}\hat{\sigma}_{yy2} + \omega_{z1}\hat{m}_{yz2} - \hat{\sigma}_{yx1}u_{x2} - \hat{\sigma}_{yy1}u_{y2} - \hat{m}_{yz1}\omega_{z2})\mathrm{d}x \tag{6}$$

where $\mathbf{J}$ is the unit symplectic matrix

$$\mathbf{J} = \begin{bmatrix} 0 & \mathbf{I}_3 \\ -\mathbf{I}_3 & 0 \end{bmatrix} \tag{7}$$

The following expression is adopted for separation of variables

$$\boldsymbol{f}(x,y) = \boldsymbol{\Phi}(x)\xi(y) = [u_x(x), u_y(x), \omega_z(x), \hat{\sigma}_{yx}(x), \hat{\sigma}_{yy}(x), \hat{m}_{yz}(x)]^{\mathrm{T}} \xi(y) \tag{8}$$

Substituting Eq. (8) into Eq. (3) yields

$$\frac{\dfrac{\partial}{\partial y}\xi(y)}{\xi(y)} = [\mathcal{H}\boldsymbol{\Phi}(x)]\boldsymbol{\Phi}^{-1}(x) \tag{9}$$

which leads to

$$\xi(y) = \mathrm{e}^{\mu y} \tag{10}$$

and the eigen equation

$$\mathcal{H}\boldsymbol{\Phi}(x) = \mu\boldsymbol{\Phi}(x) \tag{11}$$

where μ is the eigenvalue, and $\boldsymbol{\Phi}(x)$ is the corresponding eigenvector.

2.1. Eigen-solutions of zero eigenvalue

Due to the stress-free boundary conditions, the eigen-solutions for zero eigenvalue exist and they constitute the Saint-Venant solutions [26,27]. It is interesting to note that Eq. (10) is simplified as $\xi(y)=1$ for a zero eigenvalue, which indicates the absence of decaying terms along the y-axis. The governing equations for zero eigenvalue are presented below, as

$$
\begin{cases}
\dfrac{\mathrm{d}u_y(x)}{\mathrm{d}x}-2\omega_z(x)=0\\
-\dfrac{\nu}{1-\nu}\dfrac{\mathrm{d}u_x(x)}{\mathrm{d}x}+\dfrac{(1+\nu)(1-2\nu)}{E_0(1-\nu)}\hat{\sigma}_{yy}(x)=0\\
\dfrac{1+\nu}{2E_0\ell^2}\hat{m}_{yz}(x)=0\\
-\dfrac{E_0}{1-\nu^2}\dfrac{\mathrm{d}^2u_x(x)}{\mathrm{d}x^2}-\dfrac{\nu}{1-\nu}\dfrac{\mathrm{d}\hat{\sigma}_{yy}(x)}{\mathrm{d}x}-\beta\left(\dfrac{E_0}{1-\nu^2}\dfrac{\mathrm{d}u_x(x)}{\mathrm{d}x}+\dfrac{\nu}{1-\nu}\hat{\sigma}_{yy}(x)\right)=0\\
-\dfrac{2E_0}{1+\nu}\left(\dfrac{\mathrm{d}^2u_y(x)}{\mathrm{d}x^2}-\dfrac{\mathrm{d}\omega_z(x)}{\mathrm{d}x}\right)+\dfrac{\mathrm{d}\hat{\sigma}_{yx}(x)}{\mathrm{d}x}-\beta\left[\dfrac{2E_0}{1+\nu}\left(\dfrac{\mathrm{d}u_y(x)}{\mathrm{d}x}-\omega_z(x)\right)-\hat{\sigma}_{yx}(x)\right]=0\\
-\dfrac{2E_0\ell^2}{1+\nu}\dfrac{\mathrm{d}^2\omega_z(x)}{\mathrm{d}x^2}-\beta\dfrac{2E_0\ell^2}{1+\nu}\dfrac{\mathrm{d}\omega_z(x)}{\mathrm{d}x}+\dfrac{2E_0}{1+\nu}\omega_z(x)+2\hat{\sigma}_{yx}(x)-\dfrac{2E_0}{1+\nu}\dfrac{\mathrm{d}u_y(x)}{\mathrm{d}x}=0
\end{cases}
\tag{12}
$$

The eigenvectors obtained under the homogeneous boundary conditions are

$$
\boldsymbol{f}_{0,1}^{(0)}=\boldsymbol{\Phi}_{0,1}^{(0)}=[1,0,0,0,0,0]^{\mathrm{T}},\quad \boldsymbol{f}_{0,2}^{(0)}=\boldsymbol{\Phi}_{0,2}^{(0)}=[0,1,0,0,0,0]^{\mathrm{T}} \tag{13}
$$

where superscript $(\cdot)$ represents the order of Jordan form, and subscript $0,i$ represents the i-th Jordan chain for zero eigenvalue. It is important to emphasize that the eigenvectors and the corresponding eigen-solutions in Eq. (13) share common expressions, respectively. The first-order Jordan form eigenvectors of zero eigenvalue are

$$
\boldsymbol{\mathcal{H}}\boldsymbol{\Phi}_{0,1}^{(1)}=\boldsymbol{\Phi}_{0,1}^{(0)},\quad \boldsymbol{\mathcal{H}}\boldsymbol{\Phi}_{0,2}^{(1)}=\boldsymbol{\Phi}_{0,2}^{(0)} \tag{14}
$$

from which we may obtain

$$
\boldsymbol{\Phi}_{0,1}^{(1)}=[0,-x,-1,0,0,0]^{\mathrm{T}},\quad \boldsymbol{\Phi}_{0,2}^{(1)}=[-\frac{\nu}{1-\nu}x,0,0,0,\frac{E_0}{1-\nu^2},0]^{\mathrm{T}} \tag{15}
$$

and the corresponding eigen-solutions for the first-order are established as

$$
\boldsymbol{f}_{0,1}^{(1)}=\boldsymbol{\Phi}_{0,1}^{(1)}+y\boldsymbol{\Phi}_{0,1}^{(0)}=[y,-x,-1,0,0,0]^{\mathrm{T}},\quad \boldsymbol{f}_{0,2}^{(1)}=\boldsymbol{\Phi}_{0,2}^{(1)}+y\boldsymbol{\Phi}_{0,2}^{(0)}=[-\frac{\nu}{1-\nu}x,y,0,0,\frac{E_0}{1-\nu^2},0]^{\mathrm{T}} \tag{16}
$$

Following the similar procedure presented above, the second-order Jordan form eigen-equations are derived as

$$
\boldsymbol{\mathcal{H}}\boldsymbol{\Phi}_{0,1}^{(2)}=\boldsymbol{\Phi}_{0,1}^{(1)},\quad \boldsymbol{\mathcal{H}}\boldsymbol{\Phi}_{0,2}^{(2)}=\boldsymbol{\Phi}_{0,2}^{(1)} \tag{17}
$$

where the first equation above can be solved for the eigenvector, as

$$
\boldsymbol{\Phi}_{0,1}^{(2)}=[\frac{1}{2}\frac{\nu}{1-\nu}x^2,0,0,0,-\frac{E_0}{1-\nu^2}x,-\frac{2E_0\ell^2}{1+\nu}]^{\mathrm{T}} \tag{18}
$$

However, no practical eigenvector satisfies the second equation of Eq. (17), which indicates termination of the Jordan chain. Subsequently, the eigen-solution for the first chain is deduced as

$$\boldsymbol{f}_{0,1}^{(2)}=\boldsymbol{\Phi}_{0,1}^{(2)}+y\boldsymbol{\Phi}_{0,1}^{(1)}+\frac{y^2}{2}\boldsymbol{\Phi}_{0,1}^{(0)}=[\frac{1}{2}\left(\frac{\nu}{1-\nu}x^2+y^2\right),-xy,-y,0,-\frac{E_0}{1-\nu^2}x,-\frac{2E_0\ell^2}{1+\nu}]^{\mathrm{T}} \tag{19}$$

Concerning the absence of the third-order Jordan form eigenvector, we may set

$$\boldsymbol{\Phi}_0^{(2)}=\boldsymbol{\Phi}_{0,1}^{(2)}+\zeta_0\boldsymbol{\Phi}_{0,2}^{(1)} \tag{20}$$

where ζ_0 is a constant. Following the same procedure for Eq. (17), we have

$$\boldsymbol{\mathcal{H}}\boldsymbol{\Phi}_0^{(3)}=\boldsymbol{\Phi}_0^{(2)} \tag{21}$$

with the following details:

$$\begin{cases}\dfrac{\mathrm{d}u_y(x)}{\mathrm{d}x}-2\omega_z(x)=\dfrac{\nu}{1-\nu}\left(\dfrac{1}{2}x^2-\zeta_0 x\right)\\ -\dfrac{\nu}{1-\nu}\dfrac{\mathrm{d}u_x(x)}{\mathrm{d}x}+\dfrac{(1+\nu)(1-2\nu)}{E_0(1-\nu)}\hat{\sigma}_{yy}(x)=0\\ \dfrac{1+\nu}{2E_0\ell^2}\hat{m}_{yz}(x)=0\\ -\dfrac{E_0}{1-\nu^2}\dfrac{\mathrm{d}^2u_x(x)}{\mathrm{d}x^2}-\dfrac{\nu}{1-\nu}\dfrac{\mathrm{d}\hat{\sigma}_{yy}(x)}{\mathrm{d}x}-\beta\left(\dfrac{E_0}{1-\nu^2}\dfrac{\mathrm{d}u_x(x)}{\mathrm{d}x}+\dfrac{\nu}{1-\nu}\hat{\sigma}_{yy}(x)\right)=0\\ -\dfrac{2E_0}{1+\nu}\left(\dfrac{\mathrm{d}^2u_y(x)}{\mathrm{d}x^2}-\dfrac{\mathrm{d}\omega_z(x)}{\mathrm{d}x}\right)+\dfrac{\mathrm{d}\hat{\sigma}_{yx}(x)}{\mathrm{d}x}-\beta\left[\dfrac{2E_0}{1+\nu}\left(\dfrac{\mathrm{d}u_y(x)}{\mathrm{d}x}-\omega_z(x)\right)-\hat{\sigma}_{yx}(x)\right]=-\dfrac{E_0}{1-\nu^2}(x-\zeta_0)\\ -\dfrac{2E_0\ell^2}{1+\nu}\dfrac{\mathrm{d}^2\omega_z(x)}{\mathrm{d}x^2}-\beta\dfrac{2E_0\ell^2}{1+\nu}\dfrac{\mathrm{d}\omega_z(x)}{\mathrm{d}x}+\dfrac{2E_0}{1+\nu}\omega_z(x)+2\hat{\sigma}_{yx}(x)-\dfrac{2E_0}{1+\nu}\dfrac{\mathrm{d}u_y(x)}{\mathrm{d}x}=-\dfrac{2E_0\ell^2}{1+\nu}\end{cases} \tag{22}$$

We therefore obtain ζ_0 by analyzing the fifth equation of Eq. (22) with the homogeneous boundary conditions at $x=\pm L$, as

$$\frac{2E_0}{1+\nu}\left(\frac{\partial u_y(x)}{\partial x}-\omega_z(x)\right)-\hat{\sigma}_{yx}(x)=c_1\mathrm{e}^{-\beta x}+\frac{E_0}{\beta^2(1-\nu^2)}(x\beta-\beta\zeta_0-1) \tag{23}$$

where

$$\begin{cases}\zeta_0=-\dfrac{1}{\beta}+L\coth(\beta L)\\ c_1=\dfrac{E_0 L\,\mathrm{csch}(\beta L)}{\beta(1-\nu^2)}\end{cases} \tag{24}$$

We further obtain

$$\boldsymbol{\Phi}_0^{(3)}=[0,\psi_1,\psi_2,\psi_3,0,0]^{\mathrm{T}} \tag{25}$$

and the respective eigen-solution

$$\boldsymbol{f}_0^{(3)}=\boldsymbol{\Phi}_0^{(3)}+y\boldsymbol{\Phi}_{0,1}^{(2)}+\frac{y^2}{2!}\boldsymbol{\Phi}_{0,1}^{(1)}+\frac{y^3}{3!}\boldsymbol{\Phi}_{0,1}^{(0)}+\zeta_0 y\boldsymbol{\Phi}_{0,2}^{(1)}+\zeta_0\frac{y^2}{2!}\boldsymbol{\Phi}_{0,2}^{(0)} \tag{26}$$

where

$$
\begin{cases}
\psi_1 = 2\dfrac{\phi_1}{\lambda_1}\mathrm{e}^{\lambda_1 x} + 2\dfrac{\phi_2}{\lambda_1}\mathrm{e}^{\lambda_2 x} \\
\quad -\dfrac{1}{\beta(1-\nu)}\left[\dfrac{L\,\mathrm{csch}(\beta L)}{\beta}\mathrm{e}^{-\beta x} + \left(\dfrac{\beta\nu}{3}x^3 + \dfrac{\theta_1}{2}x^2 + \theta_0 x\right)\right] + \dfrac{\nu}{1-\nu}\left(\dfrac{1}{6}x^3 - \dfrac{\zeta_0}{2}x^2\right) \\
\psi_2 = \phi_1\mathrm{e}^{\lambda_1 x} + \phi_2\mathrm{e}^{\lambda_2 x} + \dfrac{1}{2\beta(1-\nu)}\left[L\,\mathrm{csch}(\beta L)\mathrm{e}^{-\beta x} - \left(\beta\nu x^2 + \theta_1 x + \theta_0\right)\right] \\
\psi_3 = \dfrac{2E_0}{1+\nu}\left\{\phi_1\mathrm{e}^{\lambda_1 x} + \phi_2\mathrm{e}^{\lambda_2 x} + \dfrac{1}{2\beta(1-\nu)}\left[L\,\mathrm{csch}(\beta L)\mathrm{e}^{-\beta x} - \left(\beta\nu x^2 + \theta_1 x + \theta_0\right)\right]\right\} \\
\quad + \dfrac{2E_0\nu}{1-\nu^2}\left(\dfrac{1}{2}x^2 - \zeta_0 x\right) - \dfrac{E_0}{\beta(1-\nu^2)}\left[x - L\coth(\beta L) + L\,\mathrm{csch}(\beta L)\mathrm{e}^{-\beta x}\right]
\end{cases}
\tag{27}
$$

and

$$
\begin{cases}
\lambda_1 = \dfrac{-\beta\ell + \sqrt{\beta^2\ell^2 + 4}}{2\ell} \\
\lambda_2 = -\dfrac{\beta\ell + \sqrt{\beta^2\ell^2 + 4}}{2\ell} \\
\theta_1 = 2\nu - 1 + 2\ell^2\beta^2\nu - 2L\beta\nu\coth(\beta L) \\
\theta_0 = \ell^2\beta(1 + 2\nu + 2\ell^2\beta^2\nu) + L\coth(\beta L) - 2L\beta^2\ell^2\nu\coth(\beta L) \\
\phi_1 = \dfrac{2\beta L\nu\cosh(\lambda_2 L) - \beta L\,\mathrm{csch}(\beta L)\sinh[(\beta + \lambda_2)L] - \theta_1\sinh(\lambda_2 L)}{2\beta\lambda_1(1-\nu)\sinh[(\lambda_1 - \lambda_2)L]} \\
\phi_2 = \dfrac{2\beta L\nu\cosh(\lambda_1 L) - \beta L\,\mathrm{csch}(\beta L)\sinh[(\beta + \lambda_1)L] - \theta_1\sinh(\lambda_1 L)}{2\beta\lambda_2(1-\nu)\sinh[(\lambda_2 - \lambda_1)L]}
\end{cases}
\tag{28}
$$

2.2. Eigen-solutions of general eigenvalues

The eigen equation is established according to Eq. (11), which yields

$$
\begin{cases}
\dfrac{\mathrm{d}u_y(x)}{\mathrm{d}x} - 2\omega_z(x) = \mu u_x(x) \\
-\dfrac{\nu}{1-\nu}\dfrac{\mathrm{d}u_x(x)}{\mathrm{d}x} + \dfrac{(1+\nu)(1-2\nu)}{E_0(1-\nu)}\hat{\sigma}_{yy}(x) = \mu u_y(x) \\
\dfrac{1+\nu}{2E_0\ell^2}\hat{m}_{yz}(x) = \mu\omega_z(x) \\
-\dfrac{E_0}{1-\nu^2}\dfrac{\mathrm{d}^2u_x(x)}{\mathrm{d}x^2} - \dfrac{\nu}{1-\nu}\dfrac{\mathrm{d}\hat{\sigma}_{yy}(x)}{\mathrm{d}x} - \beta\left(\dfrac{E_0}{1-\nu^2}\dfrac{\mathrm{d}u_x(x)}{\mathrm{d}x} + \dfrac{\nu}{1-\nu}\hat{\sigma}_{yy}(x)\right) = \mu\hat{\sigma}_{yx}(x) \\
-\dfrac{2E_0}{1+\nu}\left(\dfrac{\mathrm{d}^2u_y(x)}{\mathrm{d}x^2} - \dfrac{\mathrm{d}\omega_z(x)}{\mathrm{d}x}\right) + \dfrac{\mathrm{d}\hat{\sigma}_{yx}(x)}{\mathrm{d}x} - \beta\left[\dfrac{2E_0}{1+\nu}\left(\dfrac{\mathrm{d}u_y(x)}{\mathrm{d}x} - \omega_z(x)\right) - \hat{\sigma}_{yx}(x)\right] = \mu\hat{\sigma}_{yy}(x) \\
-\dfrac{2E_0\ell^2}{1+\nu}\dfrac{\mathrm{d}^2\omega_z(x)}{\mathrm{d}x^2} - \beta\dfrac{2E_0\ell^2}{1+\nu}\dfrac{\mathrm{d}\omega_z(x)}{\mathrm{d}x} + \dfrac{2E_0}{1+\nu}\omega_z(x) + 2\hat{\sigma}_{yx}(x) - \dfrac{2E_0}{1+\nu}\dfrac{\mathrm{d}u_y(x)}{\mathrm{d}x} = \mu\hat{m}_{yz}(x)
\end{cases}
\tag{29}
$$

Subsequently, the general solutions can be derived in the form of

$$
\boldsymbol{\Phi} = \sum_{k=1}^{6}\mathrm{e}^{\eta_k x}[\mathcal{A}_k, \mathcal{B}_k, \mathcal{C}_k, \mathcal{D}_k, \mathcal{E}_k, \mathcal{F}_k]^{\mathrm{T}} \tag{30}
$$

where $\mathcal{A}_k$, $\mathcal{B}_k$, $\mathcal{C}_k$, $\mathcal{D}_k$, $\mathcal{E}_k$, and $\mathcal{F}_k$ are constants to be determined; and η_k (presented in Appendix A) are roots of the following characteristic polynomial established from Eq. (29), as

$$\begin{aligned}&\eta^6+3\beta\eta^5+\left[3\left(\beta^2+\mu^2\right)-\frac{1}{\ell^2}\right]\eta^4+\left[\left(\beta^2+6\mu^2\right)-\frac{2}{\ell^2}\right]\beta\eta^3\\&+\left[\beta^2\left(\mu^2\frac{3-2\nu}{1-\nu}-\frac{1}{\ell^2}\right)+\mu^2\left(3\mu^2-\frac{2}{\ell^2}\right)\right]\eta^2+\left(\frac{\beta^2\nu}{1-\nu}+3\mu^2-\frac{2}{\ell^2}\right)\beta\mu^2\eta\\&+\frac{\beta^2\mu^2\nu+\mu^4\left(\beta^2\ell^2\nu+\nu-1\right)+\ell^2\mu^6(1-\nu)}{\ell^2(1-\nu)}=0\end{aligned}\tag{31}$$

It is noted that the hexic polynomial is transformed into a cubic equation by replacing η with $\sqrt{\rho}-\beta/2$, and the roots can be solved analytically.

Besides, we can further simplify Eq. (29) to analyze the relations among the constants, as

$$\begin{cases}\dfrac{\mathrm{d}u_x(x)}{\mathrm{d}x}=-\mu\dfrac{1-\nu}{\nu}u_y(x)+\dfrac{(1+\nu)(1-2\nu)}{E_0\nu}\hat{\sigma}_{yy}(x)\\\dfrac{\mathrm{d}u_y(x)}{\mathrm{d}x}=\mu u_x(x)+2\omega_z(x)\\\dfrac{\mathrm{d}}{\mathrm{d}x}\left(\dfrac{\mathrm{d}\omega_z(x)}{\mathrm{d}x}+\beta\omega_z(x)\right)=-\dfrac{1}{\ell^2}\left[\mu u_x(x)+\omega_z(x)\right]+\dfrac{1+\nu}{E_0\ell^2}\hat{\sigma}_{yx}(x)-\mu\dfrac{1+\nu}{2E_0\ell^2}\hat{m}_{yz}(x)\\\dfrac{\mathrm{d}\hat{\sigma}_{yx}(x)}{\mathrm{d}x}=\dfrac{2E_0}{1+\nu}\left[\beta\mu u_x(x)-\mu^2\dfrac{1-\nu}{\nu}u_y(x)+\left(\dfrac{\mathrm{d}\omega_z(x)}{\mathrm{d}x}+\beta\omega_z(x)\right)\right]-\beta\hat{\sigma}_{yx}(x)+\mu\dfrac{2-3\nu}{\nu}\hat{\sigma}_{yy}(x)\\\dfrac{\mathrm{d}\hat{\sigma}_{yy}(x)}{\mathrm{d}x}=\mu\dfrac{E_0}{1-\nu^2}\left[\mu u_x(x)+\beta u_y(x)+2\omega_z(x)\right]-\mu\dfrac{\nu}{1-\nu}\hat{\sigma}_{yx}(x)-\beta\hat{\sigma}_{yy}(x)\\\hat{m}_{yz}(x)=\mu\dfrac{2E_0\ell^2}{1+\nu}\omega_z(x)\end{cases}\tag{32}$$

which results in

$$\begin{cases}\mathcal{A}_k=\dfrac{(1+\nu)\left[\beta^2\nu+\beta\eta_k+(1-\nu)(\eta_k^2+\mu^2)\right]}{E_0\ell^2\left[\nu(\eta_k(\beta+\eta_k)-\beta\mu+\mu^2)(\beta(\eta_k+\mu)+\eta_k^2+\mu^2)-(\eta_k(\beta+\eta_k)+\mu^2)^2\right]}\mathcal{F}_k\\\mathcal{B}_k=\dfrac{\nu^2(\mu^2(2\beta+\eta_k)+\eta_k(\beta+\eta_k)^2)-(\beta+\eta_k)\left(\eta_k(\beta+\eta_k)+\mu^2\right)+\beta\mu^2\nu}{E_0\ell^2\mu\left[\nu(\eta_k(\beta+\eta_k)-\beta\mu+\mu^2)(\beta(\eta_k+\mu)+\eta_k^2+\mu^2)-(\eta_k(\beta+\eta_k)+\mu^2)^2\right]}\mathcal{F}_k\\\mathcal{C}_k=\dfrac{1+\nu}{2E_0\ell^2\mu}\mathcal{F}_k\\\mathcal{D}_k=\dfrac{(\beta+\eta_k)\left[\nu(\beta+\eta_k)(\eta_k^2+\mu^2)-\eta_k(\eta_k(\beta+\eta_k)+\mu^2)\right]}{\ell^2\mu\left[\nu(\eta_k(\beta+\eta_k)-\beta\mu+\mu^2)(\beta(\eta_k+\mu)+\eta_k^2+\mu^2)-(\eta_k(\beta+\eta_k)+\mu^2)^2\right]}\mathcal{F}_k\\\mathcal{E}_k=-\dfrac{(\beta+\eta_k)\left[\beta\eta_k+(1-\nu)(\eta_k^2+\mu^2)\right]}{\ell^2\left[\nu(\eta_k(\beta+\eta_k)-\beta\mu+\mu^2)(\beta(\eta_k+\mu)+\eta_k^2+\mu^2)-(\eta_k(\beta+\eta_k)+\mu^2)^2\right]}\mathcal{F}_k\end{cases}\tag{33}$$

Thus, all constants are represented by $\mathcal{F}_k$ $(k=1,2,\cdots,6)$. The characteristic equation is also

derived analytically via the homogeneous boundary conditions as

$$\begin{vmatrix} \chi_{11}\mathrm{e}^{\eta_1 L} & \chi_{12}\mathrm{e}^{\eta_2 L} & \chi_{13}\mathrm{e}^{\eta_3 L} & \chi_{14}\mathrm{e}^{\eta_4 L} & \chi_{15}\mathrm{e}^{\eta_5 L} & \chi_{16}\mathrm{e}^{\eta_6 L} \\ \chi_{11}\mathrm{e}^{-\eta_1 L} & \chi_{12}\mathrm{e}^{-\eta_2 L} & \chi_{13}\mathrm{e}^{-\eta_3 L} & \chi_{14}\mathrm{e}^{-\eta_4 L} & \chi_{15}\mathrm{e}^{-\eta_5 L} & \chi_{16}\mathrm{e}^{-\eta_6 L} \\ \chi_{21}\mathrm{e}^{\eta_1 L} & \chi_{22}\mathrm{e}^{\eta_2 L} & \chi_{23}\mathrm{e}^{\eta_3 L} & \chi_{24}\mathrm{e}^{\eta_4 L} & \chi_{25}\mathrm{e}^{\eta_5 L} & \chi_{26}\mathrm{e}^{\eta_6 L} \\ \chi_{21}\mathrm{e}^{-\eta_1 L} & \chi_{22}\mathrm{e}^{-\eta_2 L} & \chi_{23}\mathrm{e}^{-\eta_3 L} & \chi_{24}\mathrm{e}^{-\eta_4 L} & \chi_{25}\mathrm{e}^{-\eta_5 L} & \chi_{26}\mathrm{e}^{-\eta_6 L} \\ \frac{\eta_1}{\mu}\mathrm{e}^{\eta_1 L} & \frac{\eta_2}{\mu}\mathrm{e}^{\eta_2 L} & \frac{\eta_3}{\mu}\mathrm{e}^{\eta_3 L} & \frac{\eta_4}{\mu}\mathrm{e}^{\eta_4 L} & \frac{\eta_5}{\mu}\mathrm{e}^{\eta_5 L} & \frac{\eta_6}{\mu}\mathrm{e}^{\eta_6 L} \\ \frac{\eta_1}{\mu}\mathrm{e}^{-\eta_1 L} & \frac{\eta_2}{\mu}\mathrm{e}^{-\eta_2 L} & \frac{\eta_3}{\mu}\mathrm{e}^{-\eta_3 L} & \frac{\eta_4}{\mu}\mathrm{e}^{-\eta_4 L} & \frac{\eta_5}{\mu}\mathrm{e}^{-\eta_5 L} & \frac{\eta_6}{\mu}\mathrm{e}^{-\eta_6 L} \end{vmatrix} = 0 \tag{34}$$

where

$$\begin{cases} \chi_{1k} = \dfrac{\mu\left[\beta\eta_k + (1-\nu)(\eta_k^2+\mu^2)\right]}{\ell^2\left[\nu(\eta_k(\beta+\eta_k)-\beta\mu+\mu^2)(\beta(\eta_k+\mu)+\eta_k^2+\mu^2)-(\eta_k(\beta+\eta_k)+\mu^2)^2\right]} \\ \chi_{2k} = \dfrac{\eta_k(\eta_k(\beta+\eta_k)+\mu^2)-\nu(\beta+\eta_k)(\eta_k^2+\mu^2)}{\ell^2\left[\nu(\eta_k(\beta+\eta_k)-\beta\mu+\mu^2)(\beta(\eta_k+\mu)+\eta_k^2+\mu^2)-(\eta_k(\beta+\eta_k)+\mu^2)^2\right]} \end{cases} \tag{35}$$

We then obtain the eigenvalues μ_n from Eq. (34), which lead to the nontrivial solutions of $\mathcal{F}_k$. It is noted that if $\mu_n \in \mathbb{R}$, it might be a multiple eigenvalue, whose eigenvectors are constructed according to

$$\begin{cases} \boldsymbol{\mathcal{H}}\boldsymbol{\Phi}_n^{(0)} = \mu_n\boldsymbol{\Phi}_n^{(0)} \\ \boldsymbol{\mathcal{H}}\boldsymbol{\Phi}_n^{(r+1)} = \mu_n\boldsymbol{\Phi}_n^{(r+1)} + \boldsymbol{\Phi}_n^{(r)} \end{cases} \Rightarrow \left(\boldsymbol{\mathcal{H}} - \mu_n\mathbf{I}_6\right)^{r+1}\boldsymbol{\Phi}_n^{(r)} = 0 \quad (r = 0,1,\cdots,N_n-1) \tag{36}$$

which is presented in Appendix B. Hence, the eigen-solutions for general eigenvalues are

$$\boldsymbol{f}_{\mu,n}^{(i)} = \mathrm{e}^{\mu_n y}\left(\boldsymbol{\Phi}_n^{(i)} + y\boldsymbol{\Phi}_n^{(i-1)} + \cdots + \frac{y^i}{i!}\boldsymbol{\Phi}_n^{(0)}\right) \quad (i = 0,1,\cdots,N_n) \tag{37}$$

where N_n denotes multiplicity. If μ_n is a single eigenvalue (e.g., a certain $\mu_n \in \mathbb{C}\setminus\mathbb{R}$), then $N_n = 0$.

2.3. Complete solution

A complete solution of the contact problem analyzed above can be established by superposition using the eigen-solutions derived above. Hence, the symplectic expansion is

$$
\begin{aligned}
\tilde{\boldsymbol{f}} &= \boldsymbol{\mathcal{M}}\boldsymbol{f} \\
&= \sum_{n=1}^{6}\gamma_{0,n}\tilde{\boldsymbol{f}}_{0,n} + \sum_{n=1}^{\infty}\sum_{i=0}^{N_n}\left(\gamma_{\mu,n}^{\mathrm{Re},i}\mathrm{Re}\tilde{\boldsymbol{f}}_{\mu,n}^{(i)} + \gamma_{\mu,n}^{\mathrm{Im},i}\mathrm{Im}\tilde{\boldsymbol{f}}_{\mu,n}^{(i)} + \gamma_{-\mu,n}^{\mathrm{Re},i}\mathrm{Re}\tilde{\boldsymbol{f}}_{-\mu,n}^{(i)} + \gamma_{-\mu,n}^{\mathrm{Im},i}\mathrm{Im}\tilde{\boldsymbol{f}}_{-\mu,n}^{(i)}\right) \\
&\triangleq \sum_{n=1}^{\infty}\gamma_n\tilde{\boldsymbol{f}}_n
\end{aligned}
\tag{38}
$$

where $\boldsymbol{\mathcal{M}} = \mathrm{diag}[1,1,1,\mathrm{e}^{\beta x},\mathrm{e}^{\beta x},\mathrm{e}^{\beta x}]$; $\tilde{\boldsymbol{f}}_{0,n}$ $(n=1,2,\cdots,6)$ stand for eigen-solutions of zero eigenvalue; $\tilde{\boldsymbol{f}}_{\mu,n}^{(i)}$ and $\tilde{\boldsymbol{f}}_{-\mu,n}^{(i)}$ represent the ith-order eigen-solutions corresponding to the general eigenvalues μ_n and $-\mu_n$, respectively; $\mathrm{Re}(\cdot)$ and $\mathrm{Im}(\cdot)$ are the real and imaginary parts of the state vector, respectively; $\gamma_{0,n}$, $\gamma_{\mu,n}^{\mathrm{Re},i}$, $\gamma_{\mu,n}^{\mathrm{Im},i}$, $\gamma_{-\mu,n}^{\mathrm{Re},i}$, $\gamma_{-\mu,n}^{\mathrm{Im},i}$, and γ_n represent the expansion parameters. The expression in Eq. (38) indicates that for a real eigenvalue, the solution is established according to the first form where the Jordan chain should be considered for the corresponding eigenvectors. For other complex eigenvalues, the solution should be derived according to the second form.

Without loss of generality, we assume the following boundary conditions

$$
y=h,\ \begin{cases} u_x = 0 \\ u_y = 0 \\ \omega_z = 0 \end{cases};\quad y=0,\ \begin{cases} u_y = d & x\in[a,b] \\ u_x = 0 & x\in[a,b] \\ \omega_z = 0 & x\in[a,b] \\ \sigma_{yy} = 0 & x\in[-L,a]\cup[b,L] \\ \sigma_{yx} = 0 & x\in[-L,a]\cup[b,L] \\ m_{yz} = 0 & x\in[-L,a]\cup[b,L] \end{cases}
\tag{39}
$$

at $y=h$ and $y=0$ where d is the maximum indentation depth that reflects the indenter shape; and $x\in[a,b]$ is the contact area. It is noted that Eq. (40) are boundary conditions of the sticking (no-slip) indentation for a finite-sized plane rather than an infinite half-plane [31]. For the mixed boundary-value problem, the Hamiltonian mixed energy variational principal reads [32]

$$
\begin{aligned}
&\delta\left\{\int_0^h\int_{-L}^{L}\left[\boldsymbol{p}^{\mathrm{T}}\frac{\partial\boldsymbol{q}}{\partial y} - H(\boldsymbol{q},\boldsymbol{p})\right]\mathrm{d}x\mathrm{d}y - \int_{\Gamma_{q_h}}\left[\boldsymbol{p}^{\mathrm{T}}(\boldsymbol{q}-\overline{\boldsymbol{q}}_h)\right]\mathrm{d}x\right. \\
&\left. -\int_{\Gamma_{p_h}}\left[\overline{\boldsymbol{p}}_h^{\mathrm{T}}\boldsymbol{q}\right]\mathrm{d}x + \int_{\Gamma_{q_0}}\left[\boldsymbol{p}^{\mathrm{T}}(\boldsymbol{q}-\overline{\boldsymbol{q}}_0)\right]\mathrm{d}x + \int_{\Gamma_{p_0}}\left[\overline{\boldsymbol{p}}_0^{\mathrm{T}}\boldsymbol{q}\right]\mathrm{d}x\right\} = 0
\end{aligned}
\tag{40}
$$

where Γ_{q_h} denotes a boundary with known displacement $\overline{\boldsymbol{q}}_h$ at $y=h$, and the other notations represent boundaries with similar meanings. Then, Eq. (41) can be further simplified to

$$
\begin{aligned}
&\int_{\Gamma_{p_h}}\left[(\delta\boldsymbol{q})^{\mathrm{T}}(\boldsymbol{p}-\overline{\boldsymbol{p}}_h)\right]\mathrm{d}x - \int_{\Gamma_{q_h}}\left[(\delta\boldsymbol{p})^{\mathrm{T}}(\boldsymbol{q}-\overline{\boldsymbol{q}}_h)\right]\mathrm{d}x \\
&+\int_{\Gamma_{q_0}}\left[(\delta\boldsymbol{p})^{\mathrm{T}}(\boldsymbol{q}-\overline{\boldsymbol{q}}_0)\right]\mathrm{d}x - \int_{\Gamma_{p_0}}\left[(\delta\boldsymbol{q})^{\mathrm{T}}(\boldsymbol{p}-\overline{\boldsymbol{p}}_0)\right]\mathrm{d}x = 0
\end{aligned}
\tag{41}
$$

for the displacements and stresses that satisfy the canonical equation within the contact area. Substituting Eq. (38) into Eq. (42) yields

$$\begin{aligned}&\int_{\Gamma_{ph}}\left[(\sum_{i=1}^{\infty}\delta\gamma_n\boldsymbol{q}_n)^{\mathrm{T}}(\sum_{j=1}^{\infty}\gamma_m\boldsymbol{p}_m-\overline{\boldsymbol{p}}_h)\right]\mathrm{d}x-\int_{\Gamma_{qh}}\left[(\sum_{i=1}^{\infty}\delta\gamma_n\boldsymbol{p}_n)^{\mathrm{T}}(\sum_{j=1}^{\infty}\gamma_m\boldsymbol{q}_m-\overline{\boldsymbol{q}}_h)\right]\mathrm{d}x\\&+\int_{\Gamma_{q0}}\left[(\sum_{i=1}^{\infty}\delta\gamma_n\boldsymbol{p}_n)^{\mathrm{T}}(\sum_{j=1}^{\infty}\gamma_m\boldsymbol{q}_m-\overline{\boldsymbol{q}}_0)\right]\mathrm{d}x-\int_{\Gamma_{p0}}\left[(\sum_{i=1}^{\infty}\delta\gamma_n\boldsymbol{q}_n)^{\mathrm{T}}(\sum_{j=1}^{\infty}\gamma_m\boldsymbol{p}_m-\overline{\boldsymbol{p}}_0)\right]\mathrm{d}x=0\end{aligned}\tag{42}$$

By using

$$\begin{aligned}\Theta_{nm}&=\int_{\Gamma_{ph}}\left[(\boldsymbol{q}_n)^{\mathrm{T}}\boldsymbol{p}_m\right]\mathrm{d}x-\int_{\Gamma_{qh}}\left[(\boldsymbol{p}_n)^{\mathrm{T}}\boldsymbol{q}_m\right]\mathrm{d}x+\int_{\Gamma_{q0}}\left[(\boldsymbol{p}_n)^{\mathrm{T}}\boldsymbol{q}_m\right]\mathrm{d}x-\int_{\Gamma_{p0}}\left[(\boldsymbol{q}_n)^{\mathrm{T}}\boldsymbol{p}_m\right]\mathrm{d}x\\\Omega_n&=\int_{\Gamma_{ph}}\left[(\boldsymbol{q}_n)^{\mathrm{T}}\overline{\boldsymbol{p}}_h\right]\mathrm{d}x-\int_{\Gamma_{qh}}\left[(\boldsymbol{p}_n)^{\mathrm{T}}\overline{\boldsymbol{q}}_h\right]\mathrm{d}x+\int_{\Gamma_{q0}}\left[(\boldsymbol{p}_n)^{\mathrm{T}}\overline{\boldsymbol{q}}_0\right]\mathrm{d}x-\int_{\Gamma_{p0}}\left[(\boldsymbol{q}_n)^{\mathrm{T}}\overline{\boldsymbol{p}}_0\right]\mathrm{d}x\end{aligned}\tag{43}$$

then Eq. (43) may be expressed as

$$\Theta_{nm}\gamma_m=\Omega_n\tag{44}$$

If Eq. (45) is compatible, the result can be expressed in the form of

$$\gamma_i=\frac{\det\Theta_{nm}^i}{\det\Theta_{nm}}\tag{45}$$

where Θ_{nm}^i represents the matrix formed by replacing the i-th column of Θ_{nm} by the column vector Ω_n.

3. Analysis and Discussion

3.1. Distributions of eigenvalues and local phase transition

The form for complete eigen-solutions is generally linked to and determined by the distribution of eigenvalues, and thereby necessitating an analysis of the eigenvalue distribution patterns. In this instance, the length and width of the finite-sized plane are set as $2L$ and h, respectively, while Young's modulus is assumed to vary exponentially as $E_0\mathrm{e}^{\beta x}$, Poisson's ratio ν remains constant, and ℓ is the material characteristic length. In addition, the lateral boundaries are fixed, i.e., $u_x(\pm L)=0$, $u_y(\pm L)=0$, and $\omega_z(\pm L)=0$.

To elucidate the size effect, we assume $E_0=1$ (MPa), $\beta=0.1$ (mm^{-1}), $\nu=0.25$, $h=10$ (mm), and $\ell=0.01$ (mm). The distributions of eigenvalues with distinct values of L are displayed in

Fig. 2.

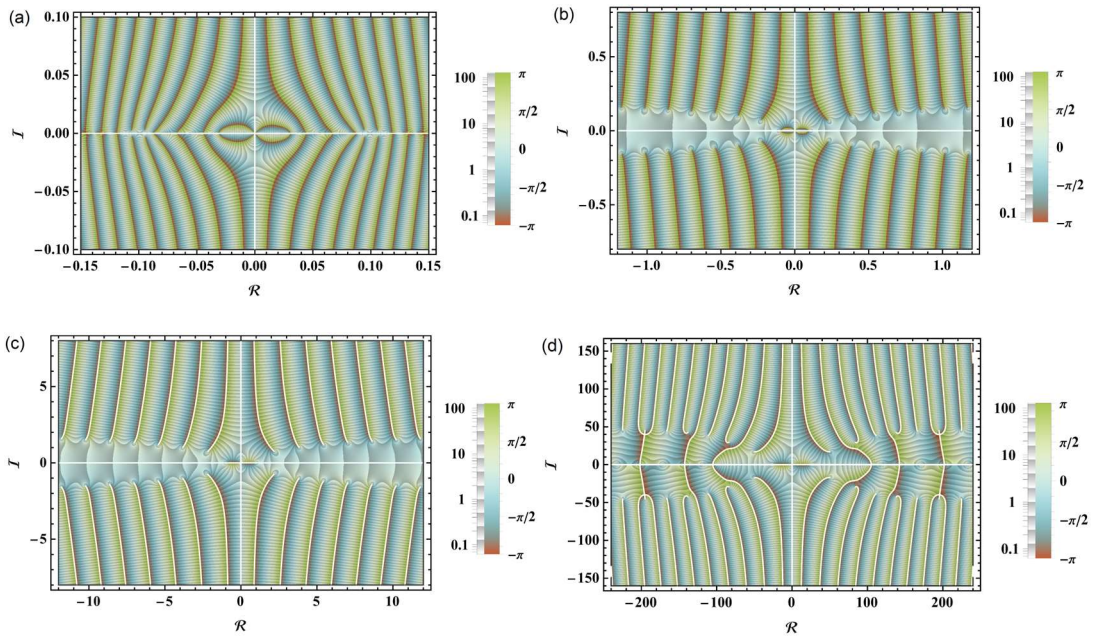

Fig. 2. Distributions of eigenvalues at different lengths of the plane: (a) $L=100$ (mm); (b) $L=10$ (mm); (c) $L=1$ (mm); and (d) $L=0.05$ (mm).

It is noteworthy that the distribution of eigenvalues remains quasi self-similar, as presented in Fig. 2 (b) and (c). Specifically, we observe that the eigenvalues are partially real rather than complex as shown in Fig. 2(d), which leads to an intriguing phenomenon, e.g., the absence of stress concentration at the corners. Therefore, the local phase transition occurs as the specimen length diminishes, which demonstrates the consequence of size effect. To elucidate, the phase transition here refers to the transition of eigenvalues in the spectrum from a periodic complex pattern to a real-complex alternating pattern. It is observable that the distance between symplectic adjoint eigenvalues and their complex conjugate counterparts along the imaginary axis progressively widens for decreasing L. Notably, at $L=100$ (mm) in Fig. 2(a), these two sets of eigenvalues come close to a nearly overlapping state, then again separate away from the coordinate origin. Actually, real eigenvalues of higher orders (far away from the coordinate origin) also emerge for the case with a large L, whereas no real eigenvalue is present in the initial few orders. This fact induces a significant impact on the eigen-solutions that are close to the coordinate origin, and it precisely forms the concept of "local" in the local phase transition.

It is evident that the scale effect is insignificant at least for $L \geq 1$ (mm) in this example, while real eigenvalues appear in the initial few orders at $L = 0.05$ (mm), suggesting that the size effect cannot be ignored at this scale. This indicates that when the size of a material (L) approaches its characteristic length (ℓ), the couple stress effect becomes obvious. However, if $L \gg \ell$, the model will reduce to a classical continuum theory.

3.2. Numerical example

A no-slip contact model is considered here where a rigid flat punch is applied to the surface of the plane exponentially graded in the x-direction, with the length and width as $2L = 2$ (m) and $h = 1$ (m), respectively. The Young's modulus at the coordinate origin, material gradient index, Poisson's ratio, and material characteristic length are set as $E_0 = 1$ (Pa), $\beta = 0.1$ (m^{-1}), $\nu = 0.25$, and $\ell = 0.01$ (m), respectively. The lateral boundary conditions are assumed to be homogeneous but distinct from that considered Section 2, i.e., we have $u_x(\pm L) = 0$, $u_y(\pm L) = 0$, and $\omega_z(\pm L) = 0$ here. While the boundary conditions at $y = h$ and $y = 0$ are referred to Eq. (40), wherein $a = 0.2$ (m), $b = 0.3$ (m), and $d = 0.02$ (m). It deserves emphasizing that the different lateral boundary conditions will lead to different characteristic equations, i.e. Eq. (34) changes. In particular, with the fixed boundary conditions, Saint-Venant solutions will not be present.

As an illustrative example, we present the result pertaining to displacements, rotation, stresses, and couple stresses as follows.

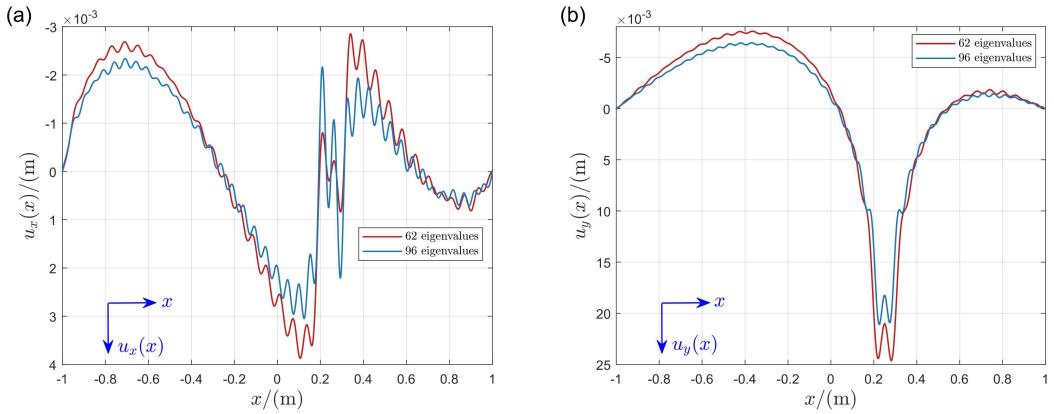

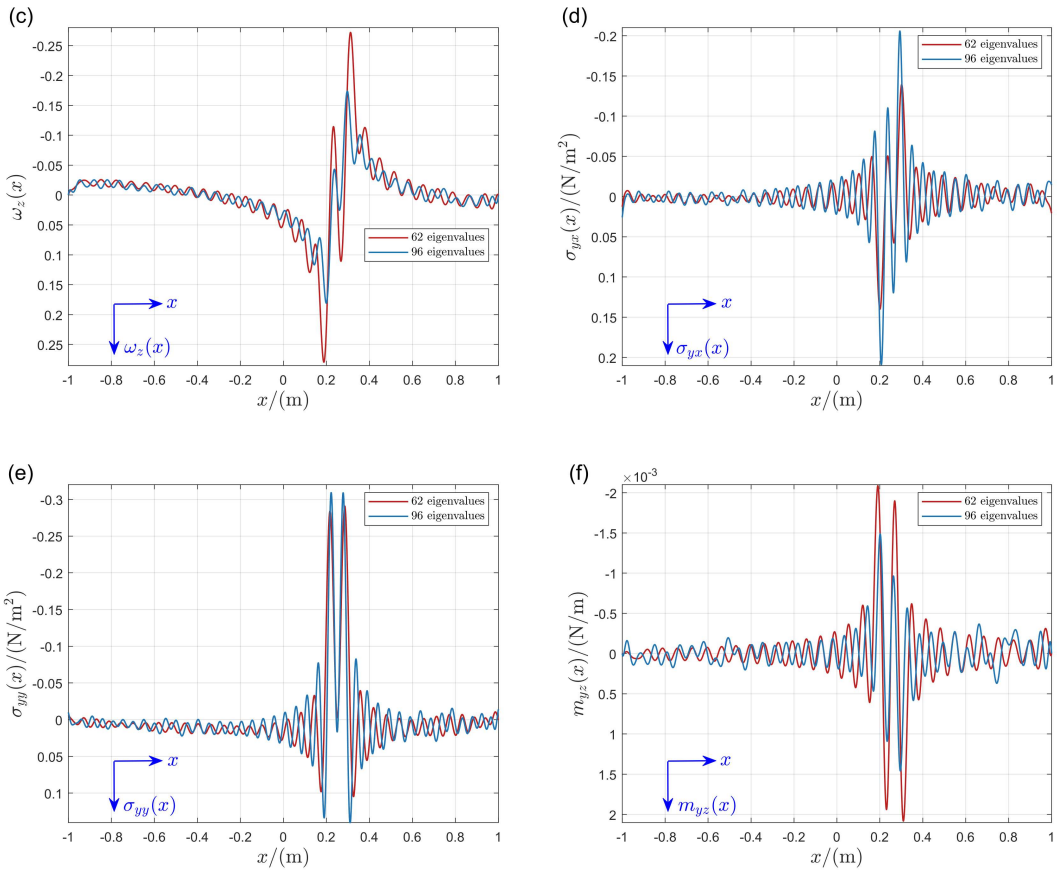

Fig. 3. Symplectic solutions for displacements, rotation, stresses, and couple stresses: (a) u_x; (b) u_y; (c) ω_z; (d) σ_{yx}; (e) σ_{yy}; and (f) m_{yz}.

It is noteworthy that a total of 62 eigenvalues are involved to obtain the first analytical solution in comparison with the second solution because real eigenvalues exist for $\Re(\mu) > 100$ (i.e., the 63$^{\mathrm{rd}}$ eigenvalue is the first real eigenvalue), as shown in Fig. 4. It is highlighted here that the real eigenvalues could be the multi-zeros of the characteristic equation, and it may lead to Jordan chain in the construction of eigen-solutions. For fixed lateral boundaries, it is noticed that the displacements at $x = \pm L$ remain zero while the stresses are nonzero, as illustrated in Fig. 3. When incorporating scale effects into our considerations, we observe notably smaller displacements along with higher stresses, which imply that the stiffness of materials undergoes an enhancement at minute sizes. Besides, the shear stress and couple stress are nonzero as compared to the result of frictionless punches [29]. However, the horizontal displacement and the rotation remain zero due to the no-slip condition. The oscillating behavior is caused by the

superposition of a finite number of eigen-solutions, which will ultimately converge if more eigenvalues are considered.

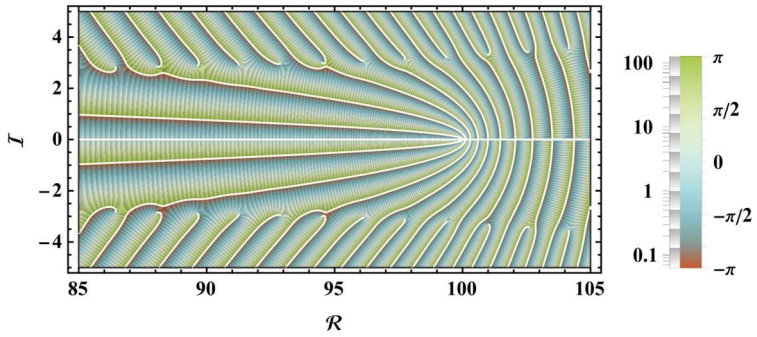

Fig. 4. Critical region where real eigenvalues exist (real axis $\Re(\mu)\in[85,105]$ and imaginary axis $\Im(\mu)\in[-5,5]$).

We may further analyze the indentation curves of size-dependent contact, as depicted in Fig. 5. The flat punch acts at a fixed position ($x\in[0.2,0.3]$ (m)) on the surface of the finite-sized plane with the length and width as $2L=2$ (m) and $h=1$ (m), respectively. Young's moduli of the homogeneous, inhomogeneous, and inhomogeneous size-dependent planes are set as $E_h=1$(Pa), $E_{ih}=1\mathrm{e}^{0.1x}$(Pa), and $E_{ihs}=1\mathrm{e}^{0.1x}$(Pa) respectively, while Poisson's ratios are all taken as $\nu=0.25$. Material characteristic length for the size-dependent case is $\ell=0.01$ (m). We observe that the inhomogeneity of the material results in a relatively steeper slope of the indentation curve at the harder side of the material. Furthermore, when the scale effect is considered, the indentation force increases, indicating the effective stiffness of the material increases.

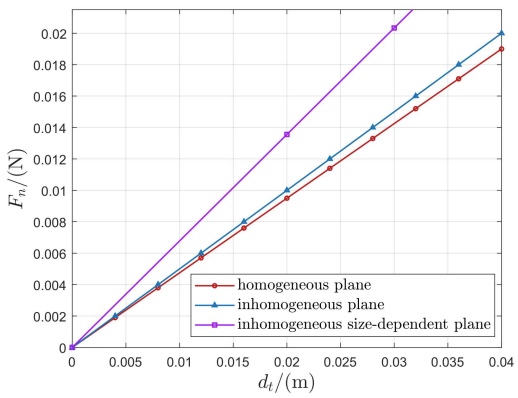

Fig. 5. Indentation curves. The flat punch acts at $x \in [0.2, 0.3](\mathrm{m})$ with the maximum indentation depth $d_M = 0.04(\mathrm{m})$.

4. Conclusions

We have established a novel symplectic framework for the couple stress theory with analytical solutions suitable for contact analysis. The contact between a no-slip rigid punch and a finite-sized plane with exponential material gradient in the horizontal direction is modeled and analyzed. Upon transforming the governing equations into the symplectic space, we obtain a new quasi-Hamiltonian operator matrix with broken symmetry in the lower-left matrix block. In this context, "symmetry breaking" arises from the inherent asymmetric stress tensor. The dual Hamiltonian transformation is derived, and the analytically obtained eigen-solutions are substituted into the symplectic expansion subsequently to determine the complete contact problem solution. It is worth noting that the eigenvalue properties should be determined beforehand to facilitate the subsequent derivation of the coefficients for superposition in distinct forms.

A highlight of this symplectic solution is the analysis of local phase transition for the distribution of the eigenvalues. The existence of real eigenvalues offers a rationale for the size effect. Additionally, the numerical example is conducted for a no-slip rigid flat punch acting on a finite-sized functionally graded plane. The symplectic methodology not only offers a powerful tool but also ushers in new possibilities for more advanced, deeper understanding and innovative solutions to complicated physical contact problems, forging a solid foundation and for future advancements in the physics of contacts.

Acknowledgments

The work was supported by the National Natural Science Foundation of China (Nos. 12192211 and 12192210), the 111 Project, PR China (No. B21034), and the specialized research projects of Huanjiang Laboratory, Zhuji, Zhejiang Province.

Disclosure statement

No potential conflict of interest was reported by the author(s).

References

[1] E. C. Aifantis, Gradient effects at macro, micro, and nano scales, J. Mech. Behav. Biomed. Mater., vol. 5, no. 3, pp. 355–375, 1994, DOI: 10.1515/JMBM.1994.5.3.355.

[2] E. Broitman, The nature of the frictional force at the macro-, micro-, and nano-scales, Friction, vol. 2, no. 1, pp. 40–46, Mar. 2014, DOI: 10.1007/s40544-014-0037-3.

[3] J. W. Judy, Microelectromechanical systems (MEMS): fabrication, design and applications, Smart. Mater. Struct., vol. 10, no. 6, p. 1115, 2001, DOI: 10.1088/0964-1726/10/6/301.

[4] Z.N. Zhao, J. Zhu, and W.Q. Chen. Size-dependent vibrations and waves in piezoelectric nanostructures: A literature review. Inter. J. Smart Nano Mater., vol. 13, no. 3, pp. 391-431, 2022, DOI: 10.1080/19475411.2022.2091058.

[5] C. Morrow, M. Lovell, and X. Ning, A JKR–DMT transition solution for adhesive rough surface contact, J. Phys. D Appl. Phys., vol. 36, no. 5, p. 534, 2003, DOI: 10.1088/0022-3727/36/5/317.

[6] R. Toupin, Elastic materials with couple-stresses, Arch. Ration. Mech. Anal., vol. 11, no. 1, pp. 385–414, 1962, DOI: 10.1007/BF00253945.

[7] R. D. Mindlin and H. Tiersten, Effects of couple-stresses in linear elasticity, Arch. Ration. Mech. Anal., vol. 11, pp. 415–448, 1962, DOI: 10.1007/BF00253946.

[8] W. Koiter, Couple-stresses in the theory of elasticity, I & II, Proc. K. Ned. Akad. Wet. Ser. B, vol. 67, pp. 17–44, 1969.

[9] E. Kröner, Elasticity theory of materials with long range cohesive forces, Int. J. Solids Struct., vol. 3, no. 5, pp. 731–742, 1967, DOI: 10.1016/0020-7683(67)90049-2.

[10] H.T. Thai, T. P. Vo, T.-K. Nguyen, and S.-E. Kim, A review of continuum mechanics models for size-dependent analysis of beams and plates, Compos. Struct., vol. 177, pp. 196–219, Oct. 2017, DOI: 10.1016/j.compstruct.2017.06.040.

[11] S.T. Liu and W.Z. Su, Effective couple-stress continuum model of cellular solids and size effects analysis, Int. J Solids Struct., vol. 46, no. 14–15, pp. 2787–2799, Jul. 2009, DOI: 10.1016/j.ijsolstr.2009.03.007.

[12] A. R. Hadjesfandiari and G. F. Dargush, Couple stress theory for solids, Int. J. Solids Struct., vol. 48, no. 18, pp. 2496–2510, Sept. 2011, DOI: 10.1016/j.ijsolstr.2011.05.002.

[13] F. Yang, A. C. M. Chong, D. C. C. Lam, and P. Tong, Couple stress based strain gradient theory for elasticity, Int. J. Solids Struct., vol. 39, no. 10, pp. 2731–2743, May 2002, DOI: 10.1016/S0020-7683(02)00152-X.

[14] R. Muki and E. Sternberg, The influence of couple-stresses on singular stress concentrations in elastic solids, Z. Angew. Math. Phys, vol. 16, no. 5, pp. 611–648, Sep. 1965, DOI: 10.1007/BF01590966.

[15] T. Zisis, Some basic contact problems in couple stress elasticity, Int. J. Solids Struct., vol. 51, pp. 2084–2095, 2014, DOI: 10.1016/j.ijsolstr.2014.02.016.

[16] P. A. Gourgiotis, Th. Zisis, and K. P. Baxevanakis, Analysis of the tilted flat punch in couple-stress elasticity, Int. J. Solids Struct., vol. 85–86, pp. 34–43, May 2016, DOI: 10.1016/j.ijsolstr.2016.01.017.

[17] P. Gourgiotis and T. Zisis, Two-dimensional indentation of microstructured solids characterized by couple-stress elasticity, J. Strain Anal. Eng. Des., vol. 51, no. 4, pp. 318–331, 2016, DOI: 10.1177/0309324715611524.

[18] T. Zisis, Anti-plane loading of microstructured materials in the context of couple stress theory of elasticity: half-planes and layers, Arch. Appl. Mech., vol. 88, no. 1–2, pp. 97–110, Feb. 2018, DOI: 10.1007/s00419-017-1277-2.

[19] T. Zisis, Burmister's problem extended to a microstructuredlayer, J. Mech. Mater. Struct., vol. 13, no. 2, pp. 203–223, May 2018, DOI: 10.2140/jomms.2018.13.203.

[20] T. Zisis, P. Gourgiotis, and F. Dal Corso, A contact problem in couple stress thermoelasticity: the indentation by a hot flat punch, Int. J. Solids Struct., vol. 63, pp. 226–239, 2015, DOI: 10.1016/j.ijsolstr.2015.03.002.

[21] Y. Wang, X. Zhang, H. Shen, J. Liu, and B. Zhang, Couple stress-based 3D contact of elastic films, Int. J. Solids Struct., vol. 191–192, pp. 449–463, May 2020, DOI: 10.1016/j.ijsolstr.2020.01.005.

[22] Y. Wang, X. Zhang, H. Shen, J. Liu, B. Zhang, and S. Xu, Three-dimensional contact analysis with couple stress elasticity, Int. J. Mech. Sci., vol. 153–154, pp. 369–379, Apr. 2019, DOI: 10.1016/j.ijmecsci.2019.02.016.

[23] C. A. Clifford and M. Seah, Modelling of nanomechanical nanoindentation measurements using an AFM or nanoindenter for compliant layers on stiffer substrates, Nanotechnology, vol. 17, no. 21, p. 5283, 2006, DOI: 10.1088/0957-4484/17/21/001.

[24] N. E. Kurland, Z. Drira, and V. K. Yadavalli, Measurement of nanomechanical properties of biomolecules using atomic force microscopy, Micron, vol. 43, no. 2–3, pp. 116–128, Feb. 2012, DOI: 10.1016/j.micron.2011.07.017.

[25] H.X. Song, L.L. Ke, and Y.S. Wang, Sliding frictional contact analysis of an elastic solid with couple stresses, Int. J. Mech. Sci., vol. 133, pp. 804–816, Nov. 2017, DOI: 10.1016/j.ijmecsci.2017.09.037.

[26] W.X. Zhong, A new systematic methodology for theory of elasticity. Dalian: Dalian University of Technology Press, 1995. (in Chinese)

[27] W. Yao, W. Zhong, and C. W. Lim, Symplectic elasticity. New Jersey: World Scientific, 2009.

[28] W. X. Zhong, G.X. Fang, and W.A. Yao, Symplectic solution for a plane couple stress problem, Adv. Mat. Res., vol. 9, pp. 143–152, 2005, DOI: 10.4028/www.scientific.net/AMR.9.143.

[29] L.Z.C. Chen and W.Q. Chen, Symplectic contact analysis of a finite-sized horizontally graded magneto-electro-elastic plane, Proc. Math. Phys. Eng. Sci., 2024, DOI: 10.1098/rspa.2024.0591.

[30] L.Z.C. Chen and W.Q. Chen, Symplectic contact analysis of a horizontally laminated magneto-electro-elastic finite specimen, Mech. Adv. Mater. Struct., 2024, DOI: 10.1080/15376494.2024.2442495.

[31] I. Argatov and G. Mishuris, Indentation testing of biological materials, vol. 91. Springer, 2018.

[32] A. Y. T. Leung and J. Zheng, Closed form stress distribution in 2D elasticity for all boundary conditions, Appl. Math. Mech.-Engl. Ed., vol. 28, no. 12, pp. 1629–1642, Dec. 2007, DOI: 10.1007/s10483-007-1210-z.

Appendix A

The roots deduced from Eq. (31) are in the form of

$$\eta_1=\frac{1}{2}\left[-\beta-\sqrt{\beta^2-4\left(\varpi_1+\varpi_2+\varpi_3\right)}\right],\qquad \eta_4=\frac{1}{2}\left[-\beta+\sqrt{\beta^2-4\left(\varpi_1+\varpi_2+\varpi_3\right)}\right]$$
$$\eta_2=\frac{1}{2}\left[-\beta-\sqrt{\beta^2-4\left(\varpi_1-\frac{1-\mathrm{i}\sqrt{3}}{2}\varpi_2-\frac{1+\mathrm{i}\sqrt{3}}{2}\varpi_3\right)}\right],\quad \eta_5=\frac{1}{2}\left[-\beta+\sqrt{\beta^2-4\left(\varpi_1-\frac{1-\mathrm{i}\sqrt{3}}{2}\varpi_2-\frac{1+\mathrm{i}\sqrt{3}}{2}\varpi_3\right)}\right] \tag{A.1}$$
$$\eta_3=\frac{1}{2}\left[-\beta-\sqrt{\beta^2-4\left(\varpi_1-\frac{1+\mathrm{i}\sqrt{3}}{2}\varpi_2-\frac{1-\mathrm{i}\sqrt{3}}{2}\varpi_3\right)}\right],\quad \eta_6=\frac{1}{2}\left[-\beta+\sqrt{\beta^2-4\left(\varpi_1-\frac{1+\mathrm{i}\sqrt{3}}{2}\varpi_2-\frac{1-\mathrm{i}\sqrt{3}}{2}\varpi_3\right)}\right]$$

where

$$\begin{aligned}
\varpi_1&=\mu^2-\frac{1}{3\ell^2}\\
\varpi_2&=\frac{\Xi}{3(1-\nu)}\\
\varpi_3&=\frac{1-\nu-3\ell^4\beta^2\mu^2\nu}{3\ell^4\Xi}\\
\Xi&=\sqrt[3]{\nu^3\left(18\beta^2\mu^2\ell^4+1\right)-3\nu^2\left(12\beta^2\mu^2\ell^4+1\right)+3\nu\left(6\beta^2\mu^2\ell^4+1\right)+3\sqrt{3}\ell^2\sqrt{\beta^2\mu^2(1-\nu)^3\nu\left(\nu\left(11\beta^2\mu^2\ell^4+2\right)+\nu^2\left(\beta^4\mu^4\ell^8-11\beta^2\mu^2\ell^4-1\right)-1\right)}-1}\Big/\ell^2
\end{aligned} \tag{A.2}$$

Appendix B

Taking $N_n=2$ for instance (i.e., the multiplicity of μ_n is 3), we can simplify Eq. (36) to

$$\begin{cases} \boldsymbol{\mathcal{H}}\boldsymbol{\Phi}_n^{(0)} = \mu_n \boldsymbol{\Phi}_n^{(0)} \\ \boldsymbol{\mathcal{H}}\boldsymbol{\Phi}_n^{(1)} = \mu_n \boldsymbol{\Phi}_n^{(1)} + \boldsymbol{\Phi}_n^{(0)} \\ \boldsymbol{\mathcal{H}}\boldsymbol{\Phi}_n^{(2)} = \mu_n \boldsymbol{\Phi}_n^{(2)} + \boldsymbol{\Phi}_n^{(1)} \end{cases} \tag{B.1}$$

The last two equations in Eq. (B.1) are usually solved by variation of the constants. Given that the eigenvectors are non-zero, we may further assume the evolution matrices $\boldsymbol{Q}_n^{(1)}$ and $\boldsymbol{Q}_n^{(2)}$ that fulfill

$$\begin{cases} \boldsymbol{\Phi}_n^{(1)} = \boldsymbol{Q}_n^{(1)} \boldsymbol{\Phi}_n^{(0)} \\ \boldsymbol{\Phi}_n^{(2)} = \boldsymbol{Q}_n^{(2)} \boldsymbol{\Phi}_n^{(1)} \end{cases} \tag{B.2}$$

The properties are obtained through modifying the first and last two relations, respectively, in Eq. (B.1) as

$$\begin{cases} \boldsymbol{Q}_n^{(1)} \boldsymbol{\mathcal{H}} \boldsymbol{\Phi}_n^{(0)} = \mu_n \boldsymbol{Q}_n^{(1)} \boldsymbol{\Phi}_n^{(0)} \\ \boldsymbol{\mathcal{H}} \boldsymbol{Q}_n^{(1)} \boldsymbol{\Phi}_n^{(0)} = \mu_n \boldsymbol{Q}_n^{(1)} \boldsymbol{\Phi}_n^{(0)} + \boldsymbol{\Phi}_n^{(0)} \end{cases} \tag{B.3}$$

and

$$\begin{cases} \boldsymbol{Q}_n^{(2)} \left(\boldsymbol{\mathcal{H}} - \mu_n \mathbf{I}_6 \right) \boldsymbol{\Phi}_n^{(1)} = \boldsymbol{Q}_n^{(2)} \boldsymbol{\Phi}_n^{(0)} \\ \left(\boldsymbol{\mathcal{H}} - \mu_n \mathbf{I}_6 \right) \boldsymbol{Q}_n^{(2)} \boldsymbol{\Phi}_n^{(1)} = \boldsymbol{\Phi}_n^{(1)} \end{cases} \tag{B.4}$$

From Eq. (B.3), we have an identity

$$\left(\left[\!\left[\boldsymbol{\mathcal{H}}, \boldsymbol{Q}_n^{(1)} \right]\!\right] - \mathbf{I}_6 \right) \boldsymbol{\Phi}_n^{(0)} = 0 \tag{B.5}$$

where $\left[\!\left[\boldsymbol{\mathcal{H}}, \boldsymbol{Q}_n^{(1)} \right]\!\right] = \boldsymbol{\mathcal{H}} \boldsymbol{Q}_n^{(1)} - \boldsymbol{Q}_n^{(1)} \boldsymbol{\mathcal{H}}$ is a commutator, and

$$\left[\!\left[\left(\boldsymbol{\mathcal{H}} - \mu_n \mathbf{I}_6 \right), \boldsymbol{Q}_n^{(2)} \right]\!\right] \boldsymbol{\Phi}_n^{(1)} = \left(\boldsymbol{Q}_n^{(1)} - \boldsymbol{Q}_n^{(2)} \right) \boldsymbol{\Phi}_n^{(0)} \tag{B.6}$$

is another identity derived from Eq. (B.4).